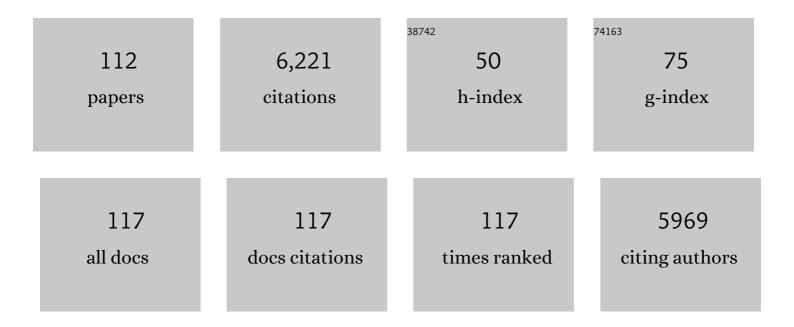
Jeffrey Catalano

List of Publications by Year in descending order

Source: https://exaly.com/author-pdf/2065559/publications.pdf Version: 2024-02-01



IFFEDEV CATALANO

#	Article	IF	CITATIONS
1	Structure and reactivity of the hydrated hematite (0001) surface. Surface Science, 2004, 573, 204-224.	1.9	279
2	Uranyl adsorption onto montmorillonite: Evaluation of binding sites and carbonate complexation. Geochimica Et Cosmochimica Acta, 2005, 69, 2995-3005.	3.9	248
3	Simultaneous inner- and outer-sphere arsenate adsorption on corundum and hematite. Geochimica Et Cosmochimica Acta, 2008, 72, 1986-2004.	3.9	220
4	Adsorption of Uranium(VI) to Manganese Oxides: X-ray Absorption Spectroscopy and Surface Complexation Modeling. Environmental Science & Technology, 2013, 47, 850-858.	10.0	187
5	Ancient Aqueous Environments at Endeavour Crater, Mars. Science, 2014, 343, 1248097.	12.6	176
6	Fluorescence spectroscopy of U(VI)-silicates and U(VI)-contaminated Hanford sediment. Geochimica Et Cosmochimica Acta, 2005, 69, 1391-1403.	3.9	136
7	Changes in Uranium Speciation through a Depth Sequence of Contaminated Hanford Sediments. Environmental Science & Technology, 2006, 40, 2517-2524.	10.0	135
8	Molecular beam epitaxial growth and properties of CoFe2O4 on MgO(001). Journal of Magnetism and Magnetic Materials, 2002, 246, 124-139.	2.3	134
9	Nanoscale Size Effects on Uranium(VI) Adsorption to Hematite. Environmental Science & Technology, 2009, 43, 1373-1378.	10.0	133
10	Spirit Mars Rover Mission: Overview and selected results from the northern Home Plate Winter Haven to the side of Scamander crater. Journal of Geophysical Research, 2010, 115, .	3.3	127
11	A hematite-bearing layer in Gale Crater, Mars: Mapping and implications for past aqueous conditions. Geology, 2013, 41, 1103-1106.	4.4	113
12	Dynamics of Chromium(VI) Removal from Drinking Water by Iron Electrocoagulation. Environmental Science & Technology, 2016, 50, 13502-13510.	10.0	107
13	Chromium speciation and mobility in a high level nuclear waste vadose zone plume. Geochimica Et Cosmochimica Acta, 2004, 68, 13-30.	3.9	103
14	Bridging arsenate surface complexes on the hematite (012) surface. Geochimica Et Cosmochimica Acta, 2007, 71, 1883-1897.	3.9	103
15	Controls on Fe(II)-Activated Trace Element Release from Goethite and Hematite. Environmental Science & Technology, 2012, 46, 1519-1526.	10.0	101
16	Weak interfacial water ordering on isostructural hematite and corundum (001) surfaces. Geochimica Et Cosmochimica Acta, 2011, 75, 2062-2071.	3.9	100
17	Termination and Water Adsorption at the α-Al2O3(012)â^'Aqueous Solution Interface. Langmuir, 2006, 22, 4668-4673.	3.5	99
18	Surface diffraction study of the hydrated hematite surface. Surface Science, 2007, 601, 460-474.	1.9	97

#	Article	IF	CITATIONS
19	Trace element cycling through iron oxide minerals during redox-driven dynamic recrystallization. Geology, 2011, 39, 1083-1086.	4.4	97
20	Spectroscopic and Diffraction Study of Uranium Speciation in Contaminated Vadose Zone Sediments from the Hanford Site, Washington State. Environmental Science & Technology, 2004, 38, 2822-2828.	10.0	96
21	Effect of Humic Acid on the Removal of Chromium(VI) and the Production of Solids in Iron Electrocoagulation. Environmental Science & Technology, 2017, 51, 6308-6318.	10.0	95
22	Molecular-Scale Structure of Uranium(VI) Immobilized with Goethite and Phosphate. Environmental Science & Technology, 2012, 46, 6594-6603.	10.0	93
23	Concentrated perchlorate at the Mars Phoenix landing site: Evidence for thin film liquid water on Mars. Geophysical Research Letters, 2010, 37, .	4.0	92
24	Analysis of uranyl-bearing phases by EXAFS spectroscopy: Interferences, multiple scattering, accuracy of structural parameters, and spectral differences. American Mineralogist, 2004, 89, 1004-1021.	1.9	90
25	Enthalpies of formation of Ce-pyrochlore, Ca0.93Ce1.00Ti2.035O7.00, U-pyrochlore, Ca1.46U4+0.23U6+0.46Ti1.85O7.00 and Gd-pyrochlore, Gd2Ti2O7: three materials relevant to the proposed waste form for excess weapons plutonium. Journal of Nuclear Materials, 2002, 303, 226-239.	2.7	84
26	CTR diffraction and grazing-incidence EXAFS study of U(VI) adsorption onto α-Al2O3 and α-Fe2O3 (11̄02) surfaces. Geochimica Et Cosmochimica Acta, 2005, 69, 3555-3572.	3.9	84
27	Interaction of Fe(II) with phosphate and sulfate on iron oxide surfaces. Geochimica Et Cosmochimica Acta, 2015, 158, 130-146.	3.9	84
28	Interfacial water structure on the (012) surface of hematite: Ordering and reactivity in comparison with corundum. Geochimica Et Cosmochimica Acta, 2007, 71, 5313-5324.	3.9	79
29	Composition and structure of nanocrystalline Fe and Mn oxide cave deposits: Implications for trace element mobility in karst systems. Chemical Geology, 2011, 284, 82-96.	3.3	78
30	Rates of Cr(VI) Generation from Cr _{<i>x</i>} Fe _{1–<i>x</i>} (OH) ₃ Solids upon Reaction with Manganese Oxide. Environmental Science & Technology, 2017, 51, 12416-12423.	10.0	78
31	Structure and oxidation state of hematite surfaces reacted with aqueous Fe(II) at acidic and neutral pH. Geochimica Et Cosmochimica Acta, 2010, 74, 1498-1512.	3.9	76
32	Effect of co-solutes on the products and solubility of uranium(VI) precipitated with phosphate. Chemical Geology, 2014, 364, 66-75.	3.3	75
33	Inner-sphere adsorption geometry of Se(IV) at the hematite (100)–water interface. Journal of Colloid and Interface Science, 2006, 297, 665-671.	9.4	74
34	Effect of Aqueous Fe(II) on Arsenate Sorption on Goethite and Hematite. Environmental Science & Technology, 2011, 45, 8826-8833.	10.0	74
35	Evidence for a Diagenetic Origin of Vera Rubin Ridge, Gale Crater, Mars: Summary and Synthesis of <i>Curiosity</i> 's Exploration Campaign. Journal of Geophysical Research E: Planets, 2020, 125, e2020JE006527.	3.6	69
36	Experimental determination of UO2(cr) dissolution kinetics: Effects of solution saturation state and pH. Journal of Nuclear Materials, 2005, 345, 206-218.	2.7	68

#	Article	IF	CITATIONS
37	Effect of phosphate on U(VI) sorption to montmorillonite: Ternary complexation and precipitation barriers. Geochimica Et Cosmochimica Acta, 2016, 175, 86-99.	3.9	68
38	Surface complexation studied via combined grazing-incidence EXAFS and surface diffraction: arsenate on hematite (0001) and (10–12). Analytical and Bioanalytical Chemistry, 2005, 383, 12-27.	3.7	66
39	Speciation of Selenium, Arsenic, and Zinc in Class C Fly Ash. Energy & Fuels, 2011, 25, 2980-2987.	5.1	63
40	Fe(II)-Mediated Reduction and Repartitioning of Structurally Incorporated Cu, Co, and Mn in Iron Oxides. Environmental Science & Technology, 2012, 46, 11070-11077.	10.0	63
41	Inhibition of Trace Element Release During Fe(II)-Activated Recrystallization of Al-, Cr-, and Sn-Substituted Goethite and Hematite. Environmental Science & Technology, 2012, 46, 10031-10039.	10.0	61
42	Structural response of phyllomanganates to wet aging and aqueous Mn(II). Geochimica Et Cosmochimica Acta, 2016, 192, 220-234.	3.9	60
43	Water ordering and surface relaxations at the hematite (110)–water interface. Geochimica Et Cosmochimica Acta, 2009, 73, 2242-2251.	3.9	58
44	Hydrated α-Fe2O3 surface structure: Role of surface preparation. Surface Science, 2007, 601, L59-L64.	1.9	57
45	Distribution and speciation of trace elements in iron and manganese oxide cave deposits. Geochimica Et Cosmochimica Acta, 2012, 91, 240-253.	3.9	57
46	Enthalpies of formation of U-, Th-, Ce-brannerite: implications for plutonium immobilization. Journal of Nuclear Materials, 2003, 320, 231-244.	2.7	56
47	Characteristics and Outcomes of Sentinel Node–Positive Breast Cancer Patients after Total Mastectomy without Axillary-Specific Treatment. Annals of Surgical Oncology, 2012, 19, 3762-3770.	1.5	56
48	High concentrations of manganese and sulfur in deposits on Murray Ridge, Endeavour Crater, Mars. American Mineralogist, 2016, 101, 1389-1405.	1.9	55
49	Structure of hydrated Zn2+ at the rutile TiO2 (110)-aqueous solution interface: Comparison of X-ray standing wave, X-ray absorption spectroscopy, and density functional theory results. Geochimica Et Cosmochimica Acta, 2006, 70, 4039-4056.	3.9	52
50	Effect of Reaction Pathway on the Extent and Mechanism of Uranium(VI) Immobilization with Calcium and Phosphate. Environmental Science & Technology, 2016, 50, 3128-3136.	10.0	52
51	Synthesis and structural characterization of ferrous trioctahedral smectites: Implications for clay mineral genesis and detectability on Mars. Journal of Geophysical Research E: Planets, 2015, 120, 1119-1140.	3.6	50
52	Thermodynamic and mass balance constraints on ironâ€bearing phyllosilicate formation and alteration pathways on early Mars. Journal of Geophysical Research E: Planets, 2013, 118, 2124-2136.	3.6	49
53	On the use of CCD area detectors for high-resolution specular X-ray reflectivity. Journal of Synchrotron Radiation, 2006, 13, 293-303.	2.4	47
54	Metal Release and Speciation Changes during Wet Aging of Coal Fly Ashes. Environmental Science & Technology, 2012, 46, 11804-11812.	10.0	46

#	Article	IF	CITATIONS
55	Competitive and Cooperative Effects during Nickel Adsorption to Iron Oxides in the Presence of Oxalate. Environmental Science & Technology, 2017, 51, 9792-9799.	10.0	46
56	Engineering Nanoscale Iron Oxides for Uranyl Sorption and Separation: Optimization of Particle Core Size and Bilayer Surface Coatings. ACS Applied Materials & amp; Interfaces, 2017, 9, 13163-13172.	8.0	44
57	Transport of U(VI) through sediments amended with phosphate to induce in situ uranium immobilization. Water Research, 2015, 69, 307-317.	11.3	43
58	Engineered manganese oxide nanocrystals for enhanced uranyl sorption and separation. Environmental Science: Nano, 2015, 2, 500-508.	4.3	43
59	Reductive transformations of layered manganese oxides by small organic acids and the fate of trace metals. Geochimica Et Cosmochimica Acta, 2019, 250, 149-172.	3.9	41
60	Relaxations and Interfacial Water Ordering at the Corundum (110) Surface. Journal of Physical Chemistry C, 2010, 114, 6624-6630.	3.1	40
61	Smectite deposits in Marathon Valley, Endeavour Crater, Mars, identified using CRISM hyperspectral reflectance data. Geophysical Research Letters, 2016, 43, 4885-4892.	4.0	39
62	Phosphate-Induced Immobilization of Uranium in Hanford Sediments. Environmental Science & Technology, 2016, 50, 13486-13494.	10.0	37
63	Impact of Mn(II)-Manganese Oxide Reactions on Ni and Zn Speciation. Environmental Science & Technology, 2017, 51, 3187-3196.	10.0	37
64	Chlorate as a Potential Oxidant on Mars: Rates and Products of Dissolved Fe(II) Oxidation. Journal of Geophysical Research E: Planets, 2019, 124, 2893-2916.	3.6	33
65	Understanding the Roles of Dissolution and Diffusion in Cr(OH) ₃ Oxidation by δ-MnO ₂ . ACS Earth and Space Chemistry, 2019, 3, 357-365.	2.7	33
66	Mars Reconnaissance Orbiter and Opportunity observations of the Burns formation: Crater hopping at Meridiani Planum. Journal of Geophysical Research E: Planets, 2015, 120, 429-451.	3.6	30
67	Oxidative Alteration of Ferrous Smectites and Implications for the Redox Evolution of Early Mars. Journal of Geophysical Research E: Planets, 2017, 122, 2469-2488.	3.6	28
68	The quench control of water estimates in convergent margin magmas. American Mineralogist, 2019, 104, 936-948.	1.9	26
69	Radiation field design and regional control in sentinel lymph nodeâ€positive breast cancer patients with omission of axillary dissection. Cancer, 2012, 118, 1994-2003.	4.1	25
70	The surface chemistry of sapphire-c: A literature review and a study on various factors influencing its IEP. Advances in Colloid and Interface Science, 2018, 251, 1-25.	14.7	25
71	Engineered superparamagnetic iron oxide nanoparticles for ultra-enhanced uranium separation and sensing. Journal of Materials Chemistry A, 2016, 4, 15022-15029.	10.3	24
72	Depositional and diagenetic constraints on the abundance and spatial variability of carbonate-associated sulfate. Chemical Geology, 2019, 523, 59-72.	3.3	23

#	Article	IF	CITATIONS
73	Synthesis and characterization of sodium meta-autunite, Na[UO2PO4]·3H2O. Radiochimica Acta, 2005, 93, .	1.2	22
74	Effects of Ionic Strength on Arsenate Adsorption at Aluminum Hydroxide–Water Interfaces. Soil Systems, 2018, 2, 1.	2.6	22
75	Association of Defects and Zinc in Hematite. Environmental Science & Technology, 2019, 53, 13687-13694.	10.0	20
76	Sorption and precipitation of Co(II) in Hanford sediments and alkaline aluminate solutions. Applied Geochemistry, 2005, 20, 193-205.	3.0	19
77	Insights on the Alumina–Water Interface Structure by Direct Comparison of Density Functional Simulations with X-ray Reflectivity. Journal of Physical Chemistry C, 2018, 122, 26934-26944.	3.1	19
78	Density Functional Theory and Thermodynamics Modeling of Inner-Sphere Oxyanion Adsorption on the Hydroxylated α-Al ₂ O ₃ (001) Surface. Langmuir, 2020, 36, 13166-13180.	3.5	19
79	Reduction of U(VI) on Chemically Reduced Montmorillonite and Surface Complexation Modeling of Adsorbed U(IV). Environmental Science & amp; Technology, 2022, 56, 4111-4120.	10.0	19
80	Sequestration of Sr(II) by calcium oxalate—A batch uptake study and EXAFS analysis of model compounds and reaction products. Geochimica Et Cosmochimica Acta, 2008, 72, 5055-5069.	3.9	18
81	Isotopic fractionation of Cu in plants. Chemical Geology, 2011, , .	3.3	18
82	Oxalate-Promoted Trace Metal Release from Crystalline Iron Oxides under Aerobic Conditions. Environmental Science and Technology Letters, 2017, 4, 311-315.	8.7	18
83	Impacts of Surface Site Coordination on Arsenate Adsorption: Macroscopic Uptake and Binding Mechanisms on Aluminum Hydroxide Surfaces. Langmuir, 2016, 32, 13261-13269.	3.5	17
84	Impact of dissolved oxygen and pH on the removal of selenium from water by iron electrocoagulation. Water Research, 2022, 213, 118159.	11.3	17
85	Influence of Oxalate on Ni Fate during Fe(II)-Catalyzed Recrystallization of Hematite and Goethite. Environmental Science & Technology, 2018, 52, 6920-6927.	10.0	16
86	Response of interfacial water to arsenate adsorption on corundum (0 0 1) surfaces: Effects of pH and adsorbate surface coverage. Geochimica Et Cosmochimica Acta, 2018, 239, 198-212.	3.9	16
87	Capacity of Chlorate to Oxidize Ferrous Iron: Implications for Iron Oxide Formation on Mars. Minerals (Basel, Switzerland), 2020, 10, 729.	2.0	15
88	Impact of Zn substitution on Fe(II)-induced ferrihydrite transformation pathways. Geochimica Et Cosmochimica Acta, 2022, 320, 143-160.	3.9	15
89	Probing interfacial reactions with X-ray reflectivity and X-ray reflection interface microscopy: Influence of NaCl on the dissolution of orthoclase at pOH 2 and 85°C. Geochimica Et Cosmochimica Acta, 2010, 74, 3396-3411.	3.9	14
90	Lambert albedo retrieval and analyses over Aram Chaos from OMEGA hyperspectral imaging data. Journal of Geophysical Research, 2012, 117, .	3.3	14

#	Article	IF	CITATIONS
91	Spectral and stratigraphic mapping of hydrated minerals associated with interior layered deposits near the southern wall of Melas Chasma, Mars. Icarus, 2018, 302, 62-79.	2.5	14
92	Effect of phosphate and sulfate on Ni repartitioning during Fe(II)-catalyzed Fe(III) oxide mineral recrystallization. Geochimica Et Cosmochimica Acta, 2015, 165, 62-74.	3.9	13
93	Insights into past ocean proxies from micron-scale mapping of sulfur species in carbonates. Geology, 2019, 47, 833-837.	4.4	12
94	Retrieval of Compositional Endâ€Members From Mars Exploration Rover Opportunity Observations in a Soilâ€Filled Fracture in Marathon Valley, Endeavour Crater Rim. Journal of Geophysical Research E: Planets, 2018, 123, 278-290.	3.6	11
95	Implications for the aqueous history of southwest Melas Chasma, Mars as revealed by interbedded hydrated sulfate and Fe/Mg-smectite deposits. Icarus, 2016, 271, 283-291.	2.5	10
96	The source of sulfate in brachiopod calcite: Insights from μ-XRF imaging and XANES spectroscopy. Chemical Geology, 2019, 529, 119328.	3.3	10
97	Effects of Cu(II) and Zn(II) on PbO ₂ Reductive Dissolution under Drinking Water Conditions: Short-term Inhibition and Long-term Enhancement. Environmental Science & Technology, 2021, 55, 14397-14406.	10.0	8
98	Consistent controls on trace metal micronutrient speciation in wetland soils and stream sediments. Geochimica Et Cosmochimica Acta, 2022, 317, 234-254.	3.9	8
99	Emerging investigator series: linking chemical transformations of silver and silver nanoparticles in the extracellular and intracellular environments to their bio-reactivity. Environmental Science: Nano, 2019, 6, 2948-2957.	4.3	7
100	Comparative response of interfacial water structure to pH variations and arsenate adsorption on corundum (0 1 2) and (0 0 1) surfaces. Geochimica Et Cosmochimica Acta, 2019, 246, 406-418.	3.9	7
101	Dynamic Responses of Trace Metal Bioaccessibility to Fluctuating Redox Conditions in Wetland Soils and Stream Sediments. ACS Earth and Space Chemistry, 2022, 6, 1331-1344.	2.7	7
102	Mineralization of contaminant uranium and leach rates in sediments from Hanford, Washington. Applied Geochemistry, 2010, 25, 97-104.	3.0	6
103	Resolving Configurational Disorder for Impurities in a Low-Entropy Phase. Journal of Physical Chemistry Letters, 2021, 12, 5689-5694.	4.6	6
104	Rates and Products of Iron Oxidation by Chlorate at Low Temperatures (0 to 25 °C) and Implications for Mars Geochemistry. ACS Earth and Space Chemistry, 2022, 6, 250-260.	2.7	6
105	Martian Habitability as Inferred From Landed Mission Observations. , 2018, , 77-126.		5
106	Copper availability governs nitrous oxide accumulation in wetland soils and stream sediments. Geochimica Et Cosmochimica Acta, 2022, 327, 96-115.	3.9	5
107	Fate of Metals in Fly Ash During Aging in Laboratory-Scale Ash Impoundments. Environmental Engineering Science, 2012, 29, 1085-1091.	1.6	4
108	First-principles characterisation and comparison of clean, hydrated, and defect α-Al ₂ O ₃ and α-Fe ₂ O ₃ (110) surfaces. Molecular Simulation, 2022, 48, 247-263.	2.0	4

#	Article	IF	CITATIONS
109	Redox-Driven Recrystallization of PbO ₂ . Environmental Science & Technology, 2022, 56, 7864-7872.	10.0	4
110	The future low-temperature geochemical data-scape as envisioned by the U.S. geochemical community. Computers and Geosciences, 2021, 157, 104933.	4.2	3
111	Canyon Wall and Floor Debris Deposits in Aeolis Mons, Mars. Journal of Geophysical Research E: Planets, 2022, 127, .	3.6	2
112	Effects of Phosphate Competition on Arsenate Binding to Aluminum Hydroxide Surfaces. ACS Earth and Space Chemistry, 2021, 5, 3140-3149.	2.7	1